PART I

Point Defects, Defect Aggregates, and Ordering

ATOM TRANSPORT AND PHASE SEPARATION IN IRRADIATED Cu-Ni-Fe ALLOYS

HEINRICH J. WOLLENBERGER

Hahn-Meitner-Institut Berlin, Glienicker Str. 100, 1000 Berlin 39, Germany

ABSTRACT

Radiation-induced atom transport controls phase stability under irradiation. Quantitative understanding of the latter phenomenon requires measurement of all relevant components of atom transport as well as of all quantities which characterize the concurrent phases. These requirements can be met for sufficiently simple systems. The paper gives an overview on studies by means of electron microscopy, field ion microscopy with atom probe, small angle neutron scattering, and diffusion coefficient measurements by depth profiling with dynamical secondary ion mass spectroscopy, all for samples irradiated with electrons, protons or heavy ions of Cu-Ni-Fe.

Evaluation of the data revealed detailed insights into the counteraction of precipitate dissolution by atomic mixing and re-precipitation by radiation-enhanced interdiffusion as well as into the evolution path of phase changes. In Cu-Ni-Fe the interstitial transport mechanism changes the tie-line for the alloy decomposition substantially when compared with the unirradiated case. Proton irradiation to fluences above 0.1 dpa indicate evolution of long-range composition fluctuations superimposed on the periodically decomposed two-phase structure. The obtained information show the importance of a combined application of microscopic, diffraction, and direct methods for atomic transport measurements.

1. Introduction

The stability of alloy phases under irradiation has been treated in the literature in view of its various aspects [1]. In general, the radiation-induced steady state of coexisting phases may be controlled by atom transport mechanisms and defect reactions being specific for each given alloy system. The question seems yet to be open whether a few fundamental processes may dominate in controlling the steady state of many systems or system specific reactions are more important. The present paper sketches the way towards an answer with respect to the role of the fundamental processes. Do we quantitatively understand the steady state of phase mixtures observed under irradiation in terms of our knowledge of fundamental irradiation effects? The attempt is made for Cu-Ni-Fe alloys, which decompose when thermally activated into two very similar coherent fcc phases [2-5]. Irradiation with Cu^+ ions at sufficiently low temperatures dissolves the precipitates and, hence, restores the one-phase solid solution. The two-phase structure occurs only within an intermediate temperature interval [2,6].

The two fundamental processes effecting the mass transport under irradiation are the atomic mixing due to recoil impact and thermal spike activation and the radiation-enhanced diffusion. The atomic mixing quoted here is observed at low irradiation temperatures such that thermally activated defect migration outside the cascade volume is suppressed. Can the shape of the radiation altered miscibility gap of the Cu-Ni-Fe alloys quantitatively be explained solely by the two mechanisms or must defect and atomic reactions be invoked, which are specific for the alloy considered?

Mat. Res. Soc. Symp. Proc. Vol. 138. ©1989 Materials Research Society

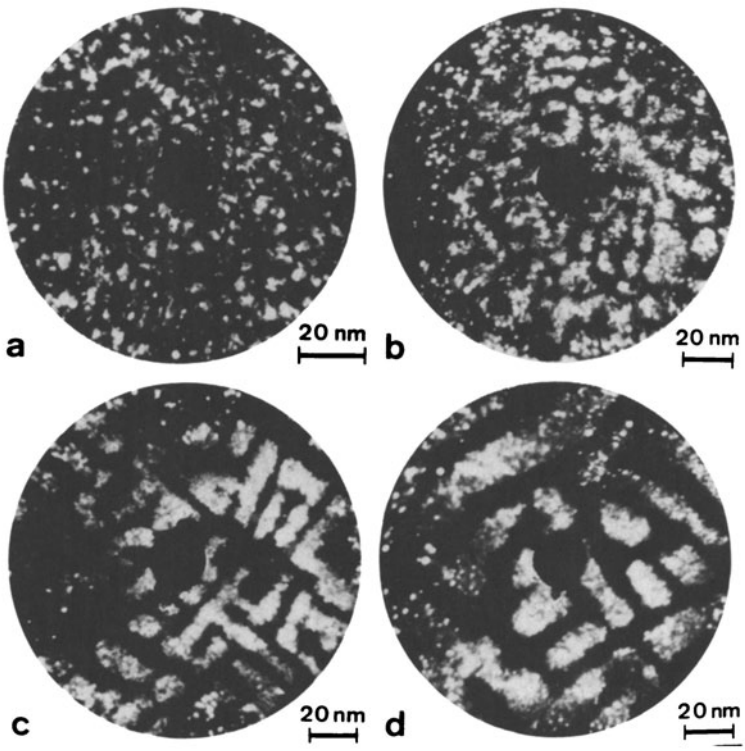

Fig. 1: FIM images for Cu-48.at%Ni-8at.%Fe annealed at 773 K for 1 h (a), 10 h (b), 100 h (c) and 1000 h (d). Bright contrast indicates Ni-rich phase.

The question was studied by determining all the required data on diffusion coefficients, steady state phase boundaries and morphologies. The detailed results have been described in ref. [6]. In the following, the main points are gathered with emphasis on showing the use of various complementary methods of analysis in order to arrive at the minimum data set necessary for answering the above quoted questions.

2. Radiation-Induced Closure of the Miscibility Gap towards Lower Temperatures

The Cu-Ni-Fe alloys of the selected compositions decompose below 900 K into two coherent fcc phases. Figs. 1 and 2 show FIM images and SANS curves for given states of ageing. As a measure for the precipitate size we use the wavelength λ of the periodic arrangement of the two phases forming {100} planes. Fig. 3 shows the time evolution of this quantity for thermally aged and for p^+-irradiated samples at the given temperature. The enhancement of the coarsening rate is obvious. Such measurements were performed at different temperatures. From the well-known interdiffusion coefficient governing the coarsening of these alloys and data as in Fig. 3, the radia-

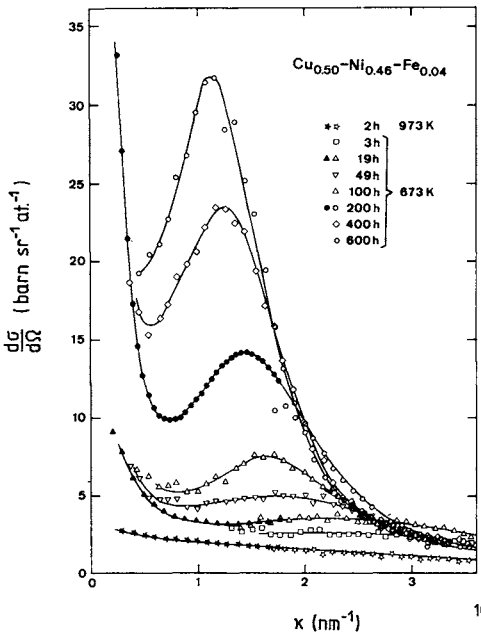

Fig. 2: SANS curves for the alloy and heat treatments indicated.

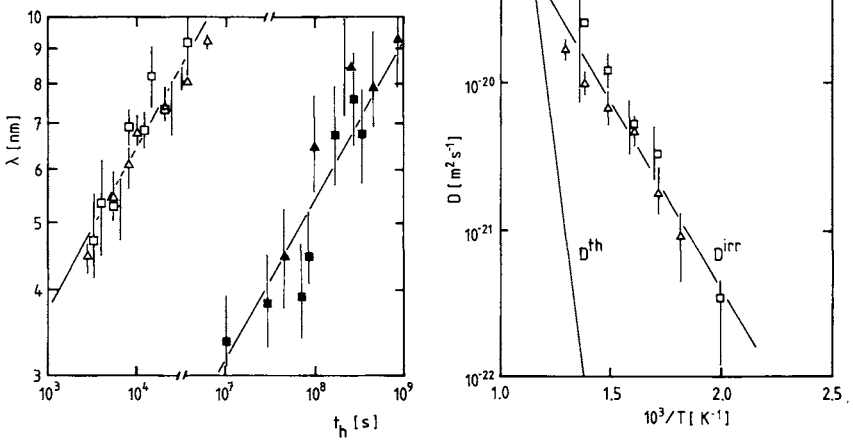

Fig. 3: Coarsening as measured by the decomposition wave length λ for proton irradiated (open symbols) and aged (full symbols) Cu-Ni-Fe alloys with the compositions like in fig. 1 (triangles) and in fig. 2 (squares). The data taken at different temperatures are scaled to 623 K [6].

Fig. 4: Interdiffusion coefficient for Cu-Ni-Fe alloys with 8at.%Fe (triangles) and 4at.%Fe (squares) as derived from coarsening kinetics (see fig. 3). D^{th} gives thermal behavior.

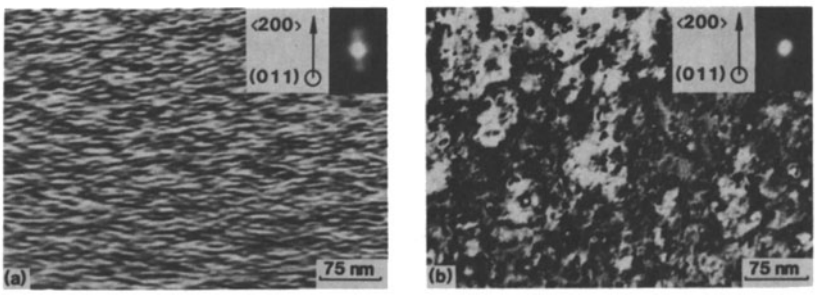

Fig. 5: TEM images of the alloy as in fig. 1 aged at 773 K (a) and subsequently irradiated at 673 K with 300 keV Cu^+ ions to 0.5 dpa (b).

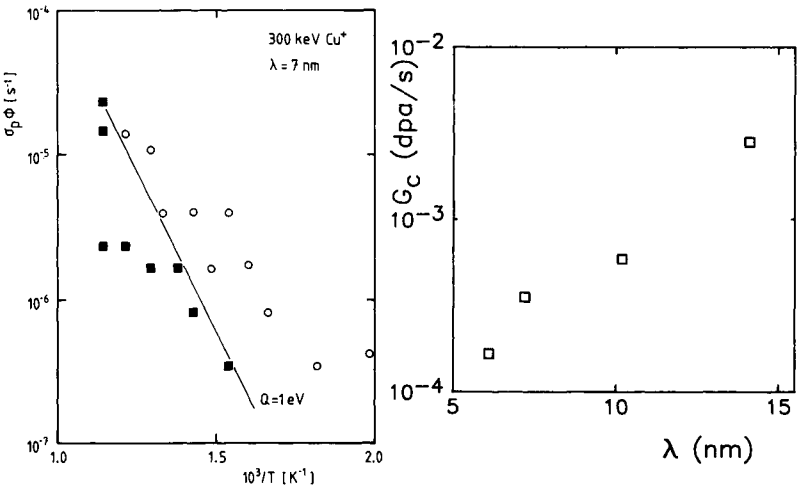

Fig. 6: Map of stability tests for the decomposed alloy with 8at.%Fe (see fig. 1). Full symbols indicate no detectable irradiation influence, open ones precipitate dissolution after 300 keV Cu^+ ion irradiation to 0.5 dpa. Ordinate represents recoil rate for primary knock-ons above 4 keV.

Fig. 7: Dependence of the primary displacement rate critical for precipitate dissolution on decomposition wave length for the alloy containing 8at.%Fe (see fig. 1) at 673 K.

tion-enhanced interdiffusion coefficient shown in Fig. 4 was derived. The question of the defect annihilation regime was studied by measuring the dependence of the interdiffusion coefficient on the displacement rate. An approximate square root dependence was found indicating recombination to dominate. For the 2 MeV p^+-irradiation and the actual sink density, atomic mixing can be neglected with respect to radiation-enhanced diffusion. Cor-

respondingly, the precipitate dissolution rate can be neglected with regard to the precipitate formation and coarsening. Even at the lowest investigated temperatures and for the highest applied fluences, p^+-irradiation-induced precipitate dissolution could not be observed.

The situation is different for 300 keV Cu^+ ion irradiation for which the mixing coefficient normalized to the displacement rate as well as the displacement rate itself are much larger than those for the p^+-irradiation. Consequently, dissolution can be observed at sufficiently low temperatures (Fig. 5). Fig. 6 gives the map of results from test irradiations in the displacement rate versus 1/T plot. The rate $\sigma_D\Phi$ represents the primary collision rate for recoil energies above 4 keV, which is taken as the cascade production rate effective for precipitate dissolution. The straight line marks the steady state phase boundary according to model calculations [7] as fitted to the data. For the quantitative explanation of the boundary in Fig. 6, in addition to the interdiffusion coefficient (Fig. 5), the mixing coefficient responsible for the precipitate dissolution must be known. It is derived from direct diffusion coefficient measurements. They have been performed by dynamical SIMS analysis of diffused samples starting with a thin tracer layer embedded within a single crystal [8,9].

Comparison of the interdiffusion coefficient and the mixing coefficient at the phase boundary in Fig. 6 yields the former to be larger by a factor of 14 or more (depending on the irradiation conditions and the precipitate size) than the latter. Such a relationship contradicts the assumption of a spatially homogeneous mixing rate [10] instead of the very localized precipitate dissolution within the cascade volume. The observed factors, however, are explained by a model, which takes into account this kind of precipitate dissolution and the restoration of the dissolved region by radiation-enhanced interdiffusion [7]. No additional rate-controlling reactions at the precipitate boundary were invoked. This model predicts a strong influence of the cascade size on the position of the phase boundary in the displacement rate versus 1/T diagram (Fig. 6).

The influence of the precipitate size has been studied with the result shown in Fig. 7. The boundary displacement rate G_c critical for precipitate dissolution at the given irradiation temperature is plotted versus the decomposition wavelength. The strong dependence reflects the localized action of the atomic mixing.

Thus far, the irradiation-induced phase boundary may indeed be interpreted solely by the two controlling processes atomic mixing and radiation-enhanced interdiffusion. It remains to be checked whether the latter leads to the same two-phase system as the thermal interdiffusion does. The coarsening behavior in Fig. 3 suggests such an identity, but it should be noted that the applied TEM analysis is not very sensitive to the composition of the two unmixing phases. Small variations of the tie-line might hardly be noticed. The situation is different for SANS which directly measures the structure function. Fortunately, this quantity senses even small atomic redistributions in these alloys when the neutron scattering contrast is enhanced by using Ni^{62}, which has a negative scattering length. Fig. 8 shows the dynamic scaling functions for the alloy containing 4 at.% Fe, which were obtained from the SANS curves of thermally aged and electron-irradiated samples [11]. Scaling behavior is observed for either kind of treatment but curves of thermally aged and irradiated samples do not scale with each other. The structure function for the irradiated samples obeys the Guinier law within a more extended range and shows a less pronounced influence of the interparticle interference (weak intensity maximum). The irradiation type structure function developed even

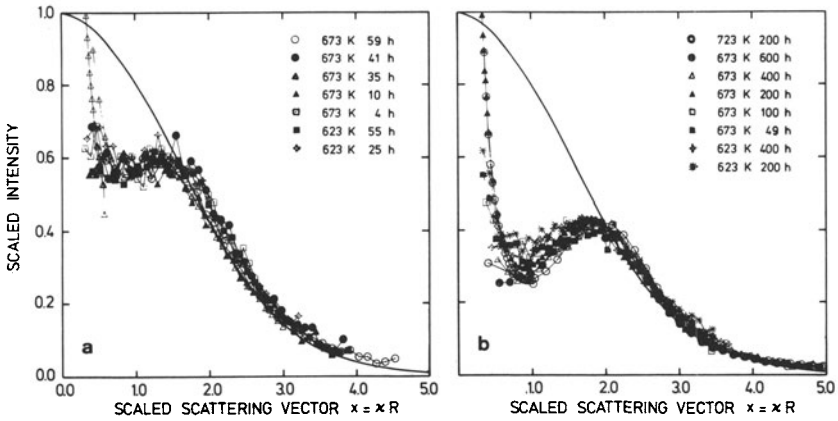

Fig. 8: Scaled SANS curves for the alloy containing 4at.%Fe (see fig. 2) after 3 MeV electron irradiation (a) at the given temperatures for the given times and after ageing (b). The solid curves represent the Guinier approximation.

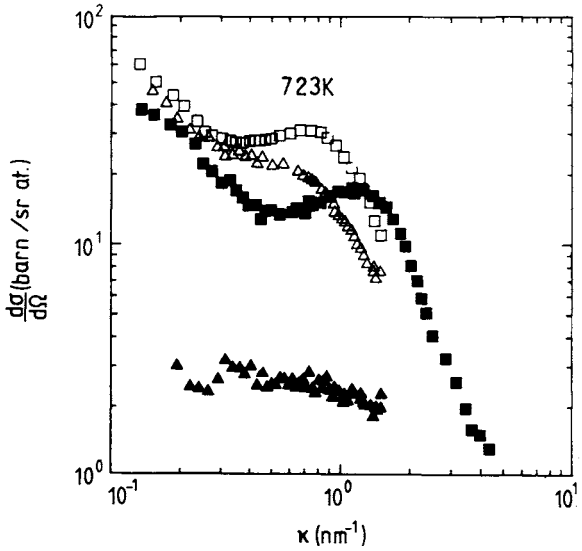

Fig. 9: SANS curves for the alloy as in fig. 1 after ageing for 50 h (full squares), electron irradiation to 7 x 10^{-4} dpa (open triangles) and ageing (50 h) plus irradiation (4 x 10^{-3} dpa) (open squares). Full triangles give quenched state.

when the irradiation temperature allowed a significant contribution of thermal vacancies to the interdiffusion. An example is given in Fig. 9. Although the thermal vacancies significantly contributed to the evolution of the scattering intensity shown by the open square data points, the ir-

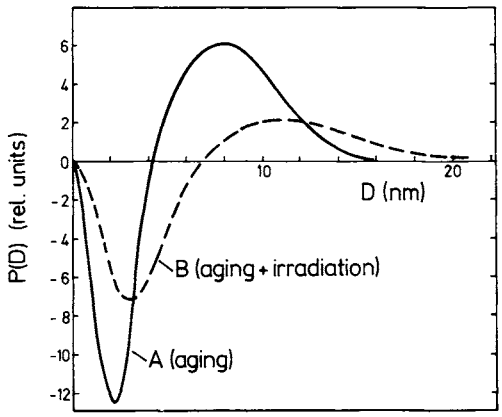

Fig. 10: Correlation functions as derived from the curves in fig. 9.

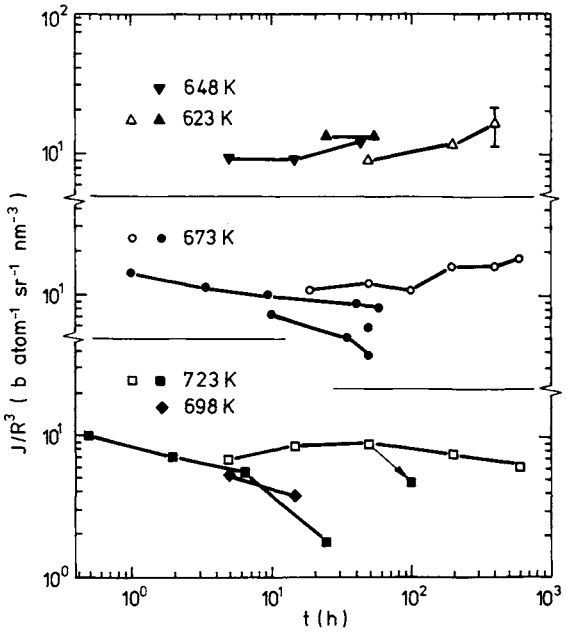

Fig. 11: Time evolution of the scaled intensity as derived from the curves in fig. 8. Open symbols indicate aged state and full symbols electron irradiated one.

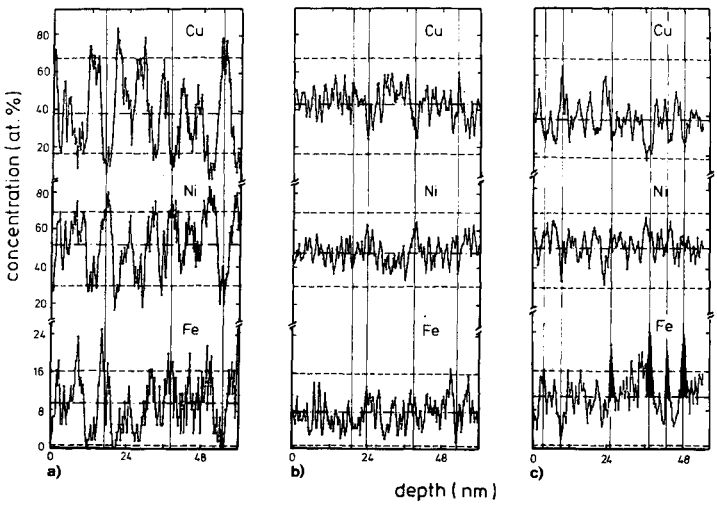

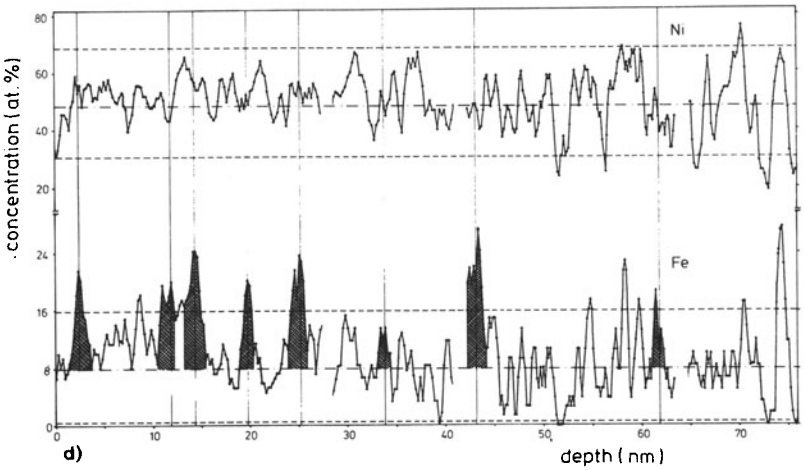

Fig. 12: Depth profiles from atom probe analysis for the alloy with 8at.%Fe (see fig. 1) after ageing (a), quenching (b) and 150 keV proton irradiation (c). Part (d) shows a selection of profile sections after electron-irradiation which demonstrate occurrence of Fe clusters not correlated to the local Ni content.